

1 Isotope Fractionation from *In Vivo* Methylmercury Detoxification in Waterbirds

2
3
4 Brett A. Poulin^{a,b*}, Sarah E. Janssen^c, Tylor J. Rosera^{c,d}, David P. Krabbenhoft^c, Collin A. Eagles-Smith^e,
5 Joshua T. Ackerman^f, A. Robin Stewart^g, Eunhee Kim^h, Zofia Baumannⁱ, Jeong-Hoon Kim^j, and Alain
6 Manceau^{k*}

7
8 ^aDepartment of Environmental Toxicology, University of California Davis, Davis, CA 95616,
9 USA (current address)

10 ^bU.S. Geological Survey, Water Mission Area, Boulder, Colorado 80303, United States

11 ^cU.S. Geological Survey, Upper Midwest Water Science Center, Middleton, Wisconsin 53562, United
12 States

13 ^dEnvironmental Chemistry and Technology Program, University of Wisconsin-Madison, Madison, WI
14 53706, USA

15 ^eU.S. Geological Survey, Forest and Rangeland Ecosystem Science Center, Corvallis, Oregon, 97331,
16 United States

17 ^fU.S. Geological Survey, Western Ecological Research Center, Dixon Field Station, Dixon, California,
18 95620, United States

19 ^gU.S. Geological Survey, Water Mission Area, Menlo Park, California, USA

20 ^hCitizens' Institute for Environmental Studies (CIES), Seoul, Korea

21 ⁱDepartment of Marine Sciences, University of Connecticut, Groton, CT 06340, USA

22 ^jDivision of Life Sciences, Korea Polar Research Institute, Incheon, Korea

23 ^kUniversity Grenoble Alpes, ISTerre, CNRS, CS 40700, 38058 Grenoble, France

24 * Corresponding authors. Tel: +1 530 754 2454. *Email address:* bapoulin@ucdavis.edu (B.A. Poulin),
25 alain.manceau@univ-grenoble-alpes.fr (A. Manceau)

27 Abstract

28 The robust application of stable mercury (Hg) isotopes for mercury source apportionment and risk
29 assessment necessitates the understanding of mass-dependent fractionation (MDF) due to internal
30 transformations within organisms. Here, we used high energy-resolution XANES spectroscopy and
31 isotope ratios of total mercury ($\delta^{202}\text{THg}$) and methylmercury ($\delta^{202}\text{MeHg}$) to elucidate the chemical
32 speciation of Hg and the resultant MDF due to internal MeHg demethylation in waterbirds. In three
33 waterbirds (Clark's grebe, Forster's tern, south polar skua), between 17-86% of the MeHg was
34 demethylated to inorganic mercury (iHg) species primarily in the liver and kidneys as Hg-tetraselenolate
35 ($\text{Hg}(\text{Sec})_4$) and minor Hg-dithiolate ($\text{Hg}(\text{SR})_2$) complexes. Tissular differences between $\delta^{202}\text{THg}$ and
36 $\delta^{202}\text{MeHg}$ correlated linearly with %iHg ($\text{Hg}(\text{Sec})_4 + \text{Hg}(\text{SR})_2$), and were interpreted to reflect a kinetic

37 isotope effect during *in vivo* MeHg demethylation. The product-reactant isotopic enrichment factor ($\epsilon_{p/r}$)
38 for the demethylation of MeHg \rightarrow Hg(Sec)₄ was $-2.2 \pm 0.1\%$. $\delta^{202}\text{MeHg}$ values were unvarying within
39 each bird regardless of Hg(Sec)₄ abundance, indicating fast internal cycling or replenishment of MeHg
40 relative to demethylation. Our findings document a universal selenium-dependent demethylation
41 reaction in birds, provide new insights on the internal transformations and cycling of MeHg and
42 Hg(Sec)₄, and allow for mathematical correction of $\delta^{202}\text{THg}$ values due to the MeHg \rightarrow Hg(Sec)₄ reaction.

43

44 **Keywords:** Mercury, demethylation, isotopes, MDF, birds

45

46 **Introduction**

47 Mercury (Hg) is a neurotoxin that impacts the health of aquatic and terrestrial animals worldwide.¹
48 Higher trophic level organisms (e.g., birds, fish, mammals) are exposed to methylmercury (MeHg)
49 through dietary sources, which is assimilated in the digestive tract, circulated in the bloodstream, and
50 retained in the protein of tissues as a MeHg-cysteine complex (MeHg-Cys).²⁻⁴ The toxicological risks of
51 MeHg to aquatic and terrestrial organisms are governed by *in vivo* transformations, inter-tissular
52 exchanges, and depuration rates and pathways of MeHg and other biologically-relevant forms of
53 mercury.¹ In birds, MeHg can be demethylated in the liver,^{5,6} depurated into feathers during molt or to
54 offspring by maternal transfer,⁷ and excreted.¹ Stable isotope ratios of mercury are a central tool for
55 ecologic risk assessment and mercury source apportionment to organisms,⁸⁻¹⁴ yet critical questions
56 remain on the isotopic fractionation of mercury by *in vivo* transformations.

57 The *in vivo* demethylation of MeHg induces mass-dependent fractionation (MDF) of mercury
58 isotopes (denoted by $\delta^{202}\text{Hg}$) as reported in birds,⁶ fish,¹⁵ and mammals.^{9,16-18} The development^{19,20} and

59 application^{16,17} of methods for species-specific mercury isotope ratio measurements show promise for
60 determining the effect of *in vivo* transformations on mercury isotope ratios. However, a chief barrier is
61 quantifying the chemical speciation of inorganic Hg (iHg) with high precision in natural tissues. High
62 energy-resolution X-ray absorption near-edge structure (HR-XANES) spectroscopy can identify and
63 quantify mixtures of biologically-relevant mercury species at sub-parts-per-million concentration.^{3,4,21–23}
64 Recent application of HR-XANES in terrestrial bird and freshwater fish tissues revealed that MeHg-Cys is
65 detoxified to a Hg-tetraselenolate (Hg(Sec)₄) complex, likely by selenoprotein P (SeP).⁴ Hg(Sec)₄ was
66 shown to be the organic precursor to nanoparticulate HgSe,⁴ which has been observed with Hg(Sec)₄ by
67 HR-XANES in marine birds²² and by normal resolution XANES in birds and mammals.^{24–26} Linking the
68 chemical speciation of iHg (that indicate specific internal reactions) and MDF of stable mercury isotopes
69 is needed to inform on the internal transformations and trafficking of mercury.

70 Here, tissues and feathers of piscivorous waterbirds from lacustrine (Clark's grebe, *Aechmophorus*
71 *clarkia*),^{4,27} estuarine (Forster's tern, *Sterna forsteri forsteri*),²⁸ and marine (south polar skua, *Stercorarius*
72 *maccormicki*) environments were measured for mercury speciation by HR-XANES spectroscopy and
73 species-specific isotope ratios. Previous research indicates internal MeHg demethylation in these
74 birds.^{4,5} Study goals were to determine the product-reactant isotopic enrichment factor ($\epsilon_{p/r}$) for the *in*
75 *vivo* detoxification of MeHg to Hg(Sec)₄ and investigate the internal cycling of biologically-relevant
76 mercury species. The findings are discussed in context of MeHg detoxification in vertebrates and
77 implications of *in vivo* MDF of mercury isotopes on environmental isotope applications.

78

79 **Materials and Methods**

80 **Biologic Tissues**

81 Tissues and feathers from three birds were analyzed including a Clark's grebe (*A. clarkia*; adult male)
82 from Lake Berryessa (California, USA; collected September 11, 2012), a Forster's tern (*S. forsteri forsteri*;
83 adult female) from the south San Francisco Bay (California, USA; collected June 13, 2018), and a south
84 polar skua (*S. maccormicki*; adult female) from Cape Hallett located in the northern Victoria Land coast
85 of the Ross Sea (Antarctica; collected November 22, 2016). The Clark's grebe and Forster's tern were
86 necropsied to obtain the following tissues: breast feather, brain, pectoral muscle, kidneys, and liver. The
87 south polar skua was necropsied to obtain the muscle, kidneys, and liver. Tissues were lyophilized and
88 homogenized. Clark's grebe tissues were analyzed previously for mercury speciation by HR-XANES and
89 mercury and selenium association with selenoproteins.⁴

90

91 **HR-XANES Measurements**

92 HR-XANES spectra of the Clark's grebe tissues are published^{4,29} and were measured identically
93 during the same experimental session on the Forster's tern and south polar skua samples. The south
94 polar skua kidney tissue was not measured by HR-XANES. Complete details are provided in the SI.
95 Briefly, mercury L₃-edge HR-XANES spectra were measured on freeze-dried samples with high-
96 reflectivity analyzer crystals³⁰ (beamline ID26, European Synchrotron Radiation Facility). Proportions of
97 Hg were quantified using least-squares fitting of data with linear combinations of diverse reference
98 spectra.^{4,21,22} The reference spectrum of MeHg-Cys was represented using the Clark's grebe breast
99 feather spectrum, which was suitable based on a spectral comparison to previously analyzed biological
100 samples with exclusively MeHg-Cys.⁴ The spectrum of Hg(Sec)₄ was determined by iterative

101 transformation factor analysis.⁴ The spectrum of Hg-dithiolate ($\text{Hg}(\text{SR})_2$) complex in biota³ was
102 represented using $\text{Hg}(\text{L-glutathione})_2$ at pH 7.4.^{31,32}

103

104 **Chemical and Isotope Analyses**

105 Details on chemical and isotope measurements are provided in the SI. Briefly, tissues and feathers
106 were measured for total mercury (THg), MeHg, and total selenium concentration.³³ Stable mercury
107 isotope ratios were measured on THg acid digests^{11,12} and resin separated MeHg fractions²⁰ of all
108 samples from the Clark's grebe and Forster's tern. For the south polar skua, THg isotope ratios were
109 measured on all tissues (muscle, kidneys, and liver) and on the MeHg fraction of the kidneys. Isotope
110 analyses were performed using a multi-collector inductively coupled plasma mass spectrometer
111 following established protocols^{34,35} on material previously exposed to the X-ray beam for HR-XANES
112 analysis, which had no effect on mercury isotope ratios ([Figure S1](#)). Delta values of MDF and mass
113 independent fractionation (MIF) are expressed as $\delta^{\text{xxx}}\text{Hg}$ and $\Delta^{\text{xxx}}\text{Hg}$, respectively, in reference to NIST
114 3133. Isotopic data on certified reference materials and standards are provided in the SI ([Table S1](#)).

115

116 **Results and Discussion**

117 **Mercury Speciation in Tissues**

118 The Hg L_3 -edge HR-XANES spectra from the three birds show distinct and consistent shifts among
119 tissues that are diagnostic of differences in mercury speciation ([Figure 1](#)). The Clark's grebe tissues
120 exhibit the most dramatic differences with mercury present as 100% MeHg-Cys in the brain (indicated
121 by the sharp near-edge peak at 12,279.8 eV unique to MeHg-Cys)^{23,36} and a progressive decrease in the
122 amplitude of the near-edge MeHg-Cys peak in the muscle, kidneys, and liver spectra. As detailed

123 previously,⁴ spectral shifts in the Clark's grebe tissues are due to an increasing percentage of mercury as
124 $\text{Hg}(\text{Sec})_4$ (0%, 11%, 59%, and 86% in brain, muscle, kidneys, and liver, respectively; [Table 1](#), [Table S2](#)). A
125 minor component of Hg-dithiolate complex ($\text{Hg}(\text{SR})_2$) is observed in the muscle (23%) and kidneys (12%)
126 ([Table 1](#)). In the Forster's tern, mercury is present solely as MeHg-Cys in the brain and muscle (100%
127 MeHg-Cys), and the kidneys and liver exhibit increasing proportions of mercury as $\text{Hg}(\text{Sec})_4$ (85% MeHg-
128 Cys + 15% $\text{Hg}(\text{Sec})_4$ and 75% MeHg-Cys + 25% $\text{Hg}(\text{Sec})_4$, respectively; [Table 1](#)). Similarly, the south polar
129 skua shows comparable differences between muscle (100% MeHg-Cys) and liver tissues (83% MeHg-Cys
130 + 17% $\text{Hg}(\text{Sec})_4$). There is no spectroscopic evidence for nanoparticulate HgSe, as observed in southern
131 giant petrel by HR-XANES.²² All tissues were modeled with high precision ([Table S2](#)) due to excellent
132 species resolution of HR-XANES (e.g., see reference spectra in [Figure 1](#)). Good agreement is observed
133 between %MeHg-Cys measured by HR-XANES and %MeHg measured by chemical measurements ([Figure](#)
134 [S2](#)), consistent with a previous comparison.⁴

135 The iHg speciation correlates to the THg concentration between bird tissues. For the Clark's grebe
136 and Forster's tern, THg concentrations of tissues (muscle, kidneys, liver) were normalized to that of the
137 brain, which exhibited 100% MeHg-Cys. A robust positive correlation is observed between % $\text{Hg}(\text{Sec})_4$
138 and the relative THg concentration of each tissue to the brain ([Figure S3](#)). Molar concentrations of Se to
139 Hg as $\text{Hg}(\text{Sec})_4$ (Se: $\text{Hg}(\text{Sec})_4$ ratio) are >4 in the Forster's tern kidneys and liver and south polar skua liver,
140 consistent with the spectroscopic evidence that tissues contain $\text{Hg}(\text{Sec})_4$ ([Figure S4](#)). The Clark's grebe
141 kidneys and liver tissues exhibit $1 < \text{Se}:\text{Hg}(\text{Sec})_4 < 4$, suggesting the co-presence of mononuclear $\text{Hg}(\text{Sec})_4$
142 complexes and disordered $\text{Hg}_x(\text{Se},\text{Sec})_y$ clusters.⁴

143

144 **Mass-Dependent Fractionation via Biotic Demethylation**

145 Mercury isotope ratios showed clear evidence for MDF in tissues that have a mixture of MeHg-Cys
146 and iHg species ($\text{Hg}(\text{Sec})_4$, $\text{Hg}(\text{SR})_2$) (Figure 2a; Table 1, Tables S3-S4). Tissular differences between
147 $\delta^{202}\text{THg}$ and $\delta^{202}\text{MeHg}$ linearly correlated with the %MeHg-Cys (and hence 100-%iHg), as determined by
148 HR-XANES (Figure 2a), suggesting that variation in $\delta^{202}\text{THg}$ is the result of mixing of two isotope
149 endmembers ($\delta^{202}\text{MeHg}$ and $\delta^{202}\text{iHg}$). For the Clark's grebe and Forster's tern, $\delta^{202}\text{THg}$ and $\delta^{202}\text{MeHg}$
150 were measured on each tissue (Table 1). For the south polar skua, $\delta^{202}\text{THg}$ was measured on the muscle
151 and liver and both $\delta^{202}\text{THg}$ and $\delta^{202}\text{MeHg}$ were measured on the kidneys. The south polar skua kidneys
152 $\delta^{202}\text{MeHg}$ ($1.25 \pm 0.02\text{‰}$) matched the muscle $\delta^{202}\text{THg}$ ($\delta^{202}\text{THg} = 1.25 \pm 0.10\text{‰}$; 100% MeHg-Cys), and
153 therefore was representative of $\delta^{202}\text{MeHg}$ in the muscle and liver. Differences between $\delta^{202}\text{THg}$ and
154 $\delta^{202}\text{MeHg}$ were greatest in the Clark's grebe tissues ($\delta^{202}\text{THg} - \delta^{202}\text{MeHg} = -1.90\text{‰}$, -1.55‰ , and -0.91‰
155 for the liver, kidneys, and muscle, respectively) followed by Foster's tern liver and kidneys tissues
156 (-0.59‰ and -0.28‰ , respectively) and the south polar skua liver (-0.45‰). In the Forster's tern, a
157 modest difference was observed between $\delta^{202}\text{THg}$ and $\delta^{202}\text{MeHg}$ values of the muscle (0.22‰) despite
158 no evidence of demethylation, and the $\delta^{202}\text{MeHg}$ of the liver was within 0.08‰ of the $\delta^{202}\text{THg}$ of the
159 muscle. Although the Clark's grebe muscle and kidneys contained varying proportions of $\text{Hg}(\text{SR})_2$ and
160 $\text{Hg}(\text{Sec})_4$, $\delta^{202}\text{Hg}$ values were consistently light compared to $\delta^{202}\text{MeHg}$ and statistically aligns with the
161 regression line between $\delta^{202}\text{THg} - \delta^{202}\text{MeHg}$ versus %MeHg-Cys (Figure 2a, Figure S5) of tissues where
162 $\text{Hg}(\text{Sec})_4$ is the dominant iHg species. Therefore, $\delta^{202}\text{iHg}$ is considered representative of the dominant
163 $\text{Hg}(\text{Sec})_4$ species.

164 Within each bird, variations of $\Delta^{199}\text{Hg}$ values and $\Delta^{199}\text{Hg}/\Delta^{201}\text{Hg}$ ratios for both the THg and the
165 MeHg fractions were largely within measurement precision regardless of mercury speciation (Figure 2b;
166 Table 1; Figure S6), consistent with previous observations of the absence of MIF during internal
167 partitioning and transformations of Hg within organisms.^{6,9,17,18} Uniformity in $\Delta^{199}\text{Hg}$ and slope of

168 $\Delta^{199}\text{Hg}/\Delta^{201}\text{Hg}$ between the MeHg and iHg species indicates photochemical demethylation occurs within
169 the food web prior to dietary assimilation of MeHg and likely reflect the bird's prey habitat and foraging
170 behavior.^{13,14,37,38}

171 We interpret isotopic differences between MeHg and $\text{Hg}(\text{Sec})_4$ to be the result of a kinetic isotope
172 effect during the *in vivo* demethylation of MeHg \rightarrow $\text{Hg}(\text{Sec})_4$. $\delta^{202}\text{MeHg}$ exhibited little variation within
173 the Clark's grebe ($-0.05 \pm 0.18\text{‰}$, average \pm standard deviation, $n=4$) and Forster's tern ($0.49 \pm 0.14\text{‰}$,
174 $n=4$) regardless of differences in mercury speciation (Table 1, Figure 2b). Therefore, the isotopic
175 fractionation of mercury in the birds behaved as an open system with an infinite reservoir of reactant
176 (i.e., MeHg). Assuming a unidirectional reaction and instantaneous product,³⁹ the product-reactant
177 isotopic enrichment factor ($\epsilon_{\text{Hg}(\text{Sec})_4/\text{MeHg}}$) was determined as the y-intercept of the linear regression
178 between $\delta^{202}\text{THg} - \delta^{202}\text{MeHg}$ versus %MeHg-Cys ($\epsilon_{\text{Hg}(\text{Sec})_4/\text{MeHg}} = -2.2 \pm 0.1\text{‰}$; slope \pm 95% confidence
179 intervals of fit; Figure 2a). The linear regression weighted each data point to measurement
180 uncertainties.⁴⁰ MDF of mercury likely occurs during demethylation of MeHg to $\text{Hg}(\text{Sec})_4$, likely by SelP.
181 SelP is rich in selenocysteine residues ($n \geq 10$ for vertebrates)^{4,41} that can facilitate MeHg
182 demethylation^{42,43} and was associated with $\text{Hg}(\text{Sec})_4$ in the Clark's grebe tissues.⁴ Notably, the Clark's
183 grebe kidneys and muscle tissues contained $\text{Hg}(\text{SR})_2$ along with $\text{Hg}(\text{Sec})_4$. Consistent MDF of tissues that
184 contain $\text{Hg}(\text{SR})_2$ and $\text{Hg}(\text{Sec})_4$ and those with only $\text{Hg}(\text{Sec})_4$ support that $\text{Hg}(\text{SR})_2$ is also a byproduct of *in*
185 *vivo* demethylation of MeHg (Figures 2a, S5), though through an unknown pathway.

186 We report the first isotopic enrichment factor for *in vivo* demethylation of MeHg by selenium in
187 vertebrates. The magnitude of $\epsilon_{\text{Hg}(\text{Sec})_4/\text{MeHg}}$ in birds ($-2.2 \pm 0.1\text{‰}$) is similar to isotopic differences
188 observed in a range of aquatic mammals (detailed below) but markedly greater than the microbial *mer*
189 pathway ($\epsilon_{p/r} = -0.40 \pm 0.20\text{‰}$).⁴⁴ In mammal tissues where species-specific isotopic ratios were
190 determined ($\delta^{202}\text{MeHg}$ and $\delta^{202}\text{THg}$),^{16,17} differences between $\delta^{202}\text{MeHg}$ and $\delta^{202}\text{iHg}$ pools were
191 estimated to range from -2.1 to $\sim -3\text{‰}$ (beluga whale and freshwater seal¹⁶ muscle versus liver, and

192 pilot whale brain tissues).¹⁷ In a study where only $\delta^{202}\text{THg}$ was measured,¹⁸ the maximum difference in
193 $\delta^{202}\text{THg}$ between muscle (~100% MeHg) and liver (~6% MeHg) in juvenile pilot whales was ~-2.3‰.
194 Consistent MDF by MeHg demethylation across birds and mammals could be explained by a universal
195 reaction mechanism involving SelP,⁴ which is central to selenium homeostasis.⁴¹ A more detailed
196 comparison of $\epsilon_{\text{Hg}(\text{Sec})_4/\text{MeHg}}$ to isotope measurements of other birds,⁶ fish,^{15,19,20} or mammals^{9,16-18} would
197 require species-specific isotope ratios and HR-XANES speciation, and knowledge of possible isotope
198 effects from poorly understood processes (e.g., biomineralization of nanoparticulate HgSe from
199 $\text{Hg}(\text{Sec})_4$).^{22,24} The expression of selenoproteins and insertion efficiency of selenocysteine residues
200 during protein translation can vary between organisms, between tissues, and based on selenium
201 availability,^{41,45} and may influence the extent of MeHg demethylation across different organisms⁶ and
202 associated isotopic fractionation in environments that differ in selenium availability. Future research
203 efforts are needed to evaluate the mechanisms and isotopic fractionation for MeHg demethylation by
204 SelP, other selenoproteins,⁴⁶ and low molecular weight selenium-containing molecule⁴⁷, and quantify
205 the variation in $\epsilon_{\text{Hg}(\text{Sec})_4/\text{MeHg}}$ across diverse organisms and environmental settings (e.g., terrestrial versus
206 marine).

207 Complementary spectroscopic and isotopic findings shed new light on the toxicokinetics of mercury
208 in birds. Regarding MeHg, tissular $\delta^{202}\text{MeHg}$ values were not influenced by the local kinetic isotopic
209 effect for the $\text{MeHg} \rightarrow \text{Hg}(\text{Sec})_4$ reaction (Figure 2b, Table 1) as would be predicted in a closed system.
210 This observation likely reflects the fast internal cycling of MeHg relative to the demethylation reaction,
211 consistent with observations in birds⁶ and marine mammals,^{16,17} and dilution of residual heavy $\delta^{202}\text{MeHg}$
212 with new dietary MeHg. The $\delta^{202}\text{MeHg}$ values of the Clark's grebe and Forster's tern feathers, which
213 fingerprint blood mercury isotope ratios during feather growth,⁴⁸ were within the narrow range of
214 tissular $\delta^{202}\text{MeHg}$ values (Table 1). Internal exchange of MeHg leading to uniform $\delta^{202}\text{MeHg}$ in the birds

215 is consistent with the dynamic nature of MeHg levels in birds due to physiological (e.g., molting, age)
216 and environmental factors (e.g., dietary exposure).^{10,27,28,49}

217 Regarding the toxicokinetics of Hg(Sec)₄, correlation between tissular concentrations of THg and
218 %Hg(Sec)₄ (Figure S3) indicates that Hg(Sec)₄ is depurated considerably slower than MeHg, consistent
219 with observations between fish muscle versus liver.⁴ It is unclear if Hg(Sec)₄ and Hg(SR)₂ in non-hepatic
220 tissues were demethylated locally or are the result of inter-tissular exchange. Inter-tissular exchange of
221 Hg(Sec)₄ or Hg(SR)₂ cannot be discounted, has been proposed in birds^{6,22} and mammals,¹⁶⁻¹⁸ and is
222 represented in toxicokinetic models,⁵⁰ but there is a lack of mechanistic studies in nature. More broadly,
223 *in vivo* demethylation of MeHg has been attributed to positive MDF between dietary MeHg and
224 organism MeHg.^{9,17,38,51,52} Quantifying the contribution of MeHg → Hg(Sec)₄ or Hg(SR)₂ on MDF between
225 dietary and organism MeHg cannot be carried out here and necessitates an improved mechanistic
226 understanding of isotopic fractionation from additional processes (e.g., ligand exchange,⁵³ Hg(Sec)₄ →
227 nanoparticulate HgSe biomineralization).²² Toxicokinetic models for mercury in birds⁵⁴ and mammals⁵⁰
228 will benefit from advancements from emerging techniques described here and elsewhere^{4,20,22} that
229 provide a foundation to understand the transformations and redistribution of biologically-relevant
230 mercury species (MeHg, Hg(SR)₂, Hg(Sec)₄, nanoparticulate HgSe).

231

232 **Implications on Environmental Applications of Stable Mercury Isotope Ratios**

233 This study demonstrates significant MDF of mercury in bird tissues due to the demethylation of
234 MeHg to primarily Hg(Sec)₄.⁴ $\delta^{202}\text{MeHg}$ values were relatively unaffected by MeHg demethylation and
235 therefore direct measurement of $\delta^{202}\text{MeHg}$ on tissues²⁰ is recommended for use of $\delta^{202}\text{Hg}$ for
236 contaminant source apportionment⁸⁻¹¹ in higher-trophic level organisms and on liver or kidney tissues
237 that are not predominantly MeHg.^{1,6,9,17,18} It is unknown if isotopically light products of *in vivo*

238 demethylation ($\text{Hg}(\text{Sec})_4$ and $\text{Hg}(\text{SR})_2$) are transferred within foodwebs (e.g., scavenging of high trophic
239 level organisms at the base of foodwebs).^{13,20} Where direct isotopic analysis of the MeHg pool is not
240 feasible, mathematical correction of $\delta^{202}\text{THg}$ using $\epsilon_{\text{Hg}(\text{Sec})_4/\text{MeHg}}$ may be warranted in determining the
241 isotopic composition of dietary MeHg sources prior to *in vivo* demethylation. When applying the
242 $\epsilon_{\text{Hg}(\text{Sec})_4/\text{MeHg}}$ ($-2.2 \pm 0.1\%$), spectroscopic characterization of tissues is encouraged under two scenarios.
243 First, in tissues with high %MeHg (e.g., >80%), HR-XANES analysis should be used to accurately quantify
244 %MeHg due to incomplete recovery of MeHg using traditional chemical techniques (Figure S2 in SI,
245 Figure S4 in Manceau et al. 2021,⁴ Figure S2 in Bolea-Fernandez et al. 2019).¹⁸ Second, in tissues with
246 low %MeHg (e.g., <30%), HR-XANES analysis is necessary to detect co-occurrence of $\text{Hg}(\text{Sec})_4$ and
247 nanoparticulate HgSe.²² It remains unknown if the biomineralization of nanoparticulate HgSe from
248 $\text{Hg}(\text{Sec})_4$ induces positive or negative MDF based on observation in marine bird⁶ and mammal tissues
249 with very low %MeHg.^{16–18,24}

250

251 **Supporting Information**

252 Descriptions of measurements; mercury isotope ratios for CRMs, standards, and samples (Table S1,
253 S3, and S4; Figure S1 and S6); HR-XANES spectra fit results (Table S2); comparison of %MeHg by HR-
254 XANES and chemical analysis (Figure S2); correlations between THg concentration and iHg speciation
255 (Figure S3); ratios of Se to Hg (Figure S4); comparison of isotope versus % $\text{Hg}(\text{Sec})_4$ by HR-XANES results
256 (Figure S5) (PDF). HR-XANES spectra (XLXS).

257

258 **Acknowledgments**

259 We thank Pieter Glatzel, Blanka Detlefs (European Synchrotron Radiation Facility), and Kathy Nagy
260 (University of Illinois at Chicago) for support during data collection on beamline ID26. We thank Mike
261 Tate, Jake Ogorek, John Pierce, and Caitlin Rumrill (U.S. Geological Survey) for assistance with mercury
262 isotope and concentration measurements. We acknowledge Brooke Hill, Jeong-Hoon Kim, and Josh
263 Ackerman for photos of the Forster's tern, south polar skua, and Clark's grebe used in the TOC art. We
264 thank Ryan Lepak (US EPA) and two anonymous reviewers for constructive feedback on the manuscript.
265 Financial support was provided to B.A.P. by the U.S. National Science Foundation under grant EAR-
266 1629698, to B.A.P., S.E.J., A.R.S., D.P.K., C.A.E., and J.T.A. by the U.S. Geological Survey (USGS)
267 Environmental Health Mission Area's Toxic Substances Hydrology and Contaminants Biology Programs,
268 and to A.R.S. by the Water Mission Area. Financial support was provided to A.M. by the French National
269 Research Agency (ANR) under grant ANR-10-EQPX-27-01 (EcoX Equipex), and to E.K. and J.H.K. by the
270 Ecosystem Structure and Function of Marine Protected Area (MPA) in Antarctica' project (PM20060),
271 funded by the Ministry of Oceans and Fisheries (20170336), Korea. Any use of trade, firm, or product
272 names is for descriptive purposes only and does not imply endorsement by the U.S. Government.

273

274 **References**

- 275 (1) Chételat, J.; Ackerman, J. T.; Eagles-Smith, C. A.; Hebert, C. E. Methylmercury exposure in wildlife:
276 A review of the ecological and physiological processes affecting contaminant concentrations and
277 their interpretation. *Sci. Total Environ.* **2020**, *711*, DOI: 10.1016/j.scitotenv.2019.135117.
- 278 (2) Harris, H. H.; Pickering, I. J.; George, G. N. The chemical form of mercury in fish. *Science* **2003**,
279 *301*, 1203, DOI: 10.1126/science.1085941.
- 280 (3) Bourdineaud, J. P.; Gonzalez-Rey, M.; Rovezzi, M.; Glatzel, P.; Nagy, K. L.; Manceau, A. Divalent
281 mercury in dissolved organic matter is bioavailable to fish and accumulates as dithiolate and
282 tetrathiolate complexes. *Environ. Sci. Technol.* **2019**, *53*, 4880-4891, DOI:
283 10.1021/acs.est.8b06579.

- 284 (4) Manceau, A.; Bourdineaud, J. P.; Oliveira, R. B.; Sarrazin, S. L. F.; Krabbenhoft, D. P.; Eagles-Smith,
285 C. A.; Ackerman, J. T.; Stewart, A. R.; Ward-Deitrich, C.; del Castillo Busto, M. E.; Goenaga-Infante,
286 H.; Wack, A.; Retegan, M.; Detlefs, B.; Glatzel, P.; Bustamante, P.; Nagy, K. L.; Poulin, B. A.
287 Demethylation of methylmercury in bird, fish, and earthworm. *Environ. Sci. Technol.* **2021**, *55*,
288 1527-1534, DOI: 10.1021/acs.est.0c04948.
- 289 (5) Eagles-Smith, C. A.; Ackerman, J. T.; Julie, Y. E. E.; Adelsbach, T. L. Mercury demethylation in
290 waterbird livers: Dose-response thresholds and differences among species. *Environ. Toxicol.*
291 *Chem.* **2009**, *28*, 568-577, DOI: 10.1897/08-245.1.
- 292 (6) Renedo, M.; Pedrero, Z.; Amouroux, D.; Cherel, Y.; Bustamante, P. Mercury Isotopes of Key
293 Tissues Document Mercury Metabolic Processes in Seabirds. *Chemosphere* **2021**, *263*, 127777,
294 DOI: 10.1016/j.chemosphere.2020.127777.
- 295 (7) Ackerman, J. T.; Herzog, M. P.; Evers, D. C.; Cristol, D. A.; Kenow, K. P.; Heinz, G. H.; Lavoie, R. A.;
296 Brasso, R. L.; Mallory, M. L.; Provencher, J. F.; Braune, B. M.; Matz, A.; Schmutz, J. A.; Eagles-
297 Smith, C. A.; Savoy, L. J.; Meyer, M. W.; Hartman, C. A. Synthesis of maternal transfer of mercury
298 in birds: Implications for altered toxicity risk. *Environ. Sci. Technol.* **2020**, *54*, 2878–2891, DOI:
299 10.1021/acs.est.9b06119.
- 300 (8) Li, M.; Schartup, A. T.; Valberg, A. P.; Ewald, J. D.; Krabbenhoft, D. P.; Yin, R.; Balcom, P. H.;
301 Sunderland, E. M. Environmental origins of methylmercury accumulated in subarctic estuarine
302 fish indicated by mercury stable isotopes. *Environ. Sci. Technol.* **2016**, *50*, 11559-11568, DOI:
303 10.1021/acs.est.6b03206.
- 304 (9) Masbou, J.; Sonke, J. E.; Amouroux, D.; Guillou, G.; Becker, P. R.; Point, D. Hg-stable isotope
305 variations in marine top predators of the western Arctic Ocean. *ACS Earth Sp. Chem.* **2018**, *2*,
306 479-490, DOI: 10.1021/acsearthspacechem.8b00017.
- 307 (10) Renedo, M.; Amouroux, D.; Pedrero, Z.; Bustamante, P.; Cherel, Y. Identification of sources and
308 bioaccumulation pathways of MeHg in subantarctic penguins: A stable isotopic investigation. *Sci.*
309 *Rep.* **2018**, *8*, DOI: 10.1038/s41598-018-27079-9.
- 310 (11) Lepak, R. F.; Janssen, S. E.; Yin, R.; Krabbenhoft, D. P.; Ogorek, J. M.; DeWild, J. F.; Tate, M. T.;
311 Holsen, T. M.; Hurley, J. P. Factors affecting mercury stable isotopic distribution in piscivorous
312 fish of the Laurentian Great Lakes. *Environ. Sci. Technol.* **2018**, *52*, 2768–2776. DOI:
313 10.1021/acs.est.7b06120.
- 314 (12) Lepak, R. F.; Hoffman, J. C.; Janssen, S. E.; Krabbenhoft, D. P.; Ogorek, J. M.; DeWild, J. F.; Tate, M.
315 T.; Babiarz, C. L.; Yin, R.; Murphy, E. W.; Engstrom, D. R.; Hurley, J. P. Mercury source changes and
316 food web shifts alter contamination signatures of predatory fish from Lake Michigan. *Proc. Natl.*
317 *Acad. Sci. U. S. A.* **2019**, *116*, 23600-23608, DOI: 10.1073/pnas.1907484116.
- 318 (13) Blum, J. D.; Drazen, J. C.; Johnson, M. W.; Popp, B. N.; Motta, L. C.; Jamieson, A. J. Mercury
319 isotopes identify near-surface marine mercury in deep-sea trench biota. *Proc. Natl. Acad. Sci.*
320 **2020**, *117*, 29292-29298, DOI: 10.1073/pnas.2012773117.
- 321 (14) Blum, J. D.; Sherman, L. S.; Johnson, M. W. Mercury isotopes in earth and environmental
322 sciences. *Annu. Rev. Earth Planet. Sci.* **2014**, *42*, 249–269, DOI: 10.1146/annurev-earth-050212-
323 124107.
- 324 (15) Rua-Ibarz, A.; Bolea-Fernandez, E.; Maage, A.; Frantzen, S.; Sanden, M.; Vanhaecke, F. Tracing

- 325 mercury pollution along the Norwegian coast via elemental, speciation, and isotopic analysis of
326 liver and muscle tissue of deep-water marine fish (*Brosme Brosme*). *Environ. Sci. Technol.* **2019**,
327 *53*, 1776-1785, DOI: 10.1021/acs.est.8b04706.
- 328 (16) Perrot, V.; Masbou, J.; Pastukhov, M. V.; Epov, V. N.; Point, D.; Bérail, S.; Becker, P. R.; Sonke, J.
329 E.; Amouroux, D. Natural Hg isotopic composition of different Hg compounds in mammal tissues
330 as a proxy for in vivo breakdown of toxic methylmercury. *Metallomics* **2016**, *8*, 170, DOI:
331 10.1039/c5mt00286a.
- 332 (17) Li, M.; Juang, C. A.; Ewald, J. D.; Yin, R.; Mikkelsen, B.; Krabbenhoft, D. P.; Balcom, P. H.;
333 Dassuncao, C.; Sunderland, E. M. Selenium and stable mercury isotopes provide new insights into
334 mercury toxicokinetics in pilot whales. *Sci. Total Environ.* **2020**, *710*, 136325, DOI:
335 10.1016/j.scitotenv.2019.136325.
- 336 (18) Bolea-Fernandez, E.; Rua-Ibarz, A.; Krupp, E. M.; Feldmann, J.; Vanhaecke, F. High-precision
337 isotopic analysis sheds new light on mercury metabolism in long-finned pilot whales
338 (*Globicephala Melas*). *Sci. Rep.* **2019**, *9*, 7262, DOI: 10.1038/s41598-019-43825-z.
- 339 (19) Masbou, J.; Point, D.; Sonke, J. E. Application of a selective extraction method for methylmercury
340 compound specific stable isotope analysis (MeHg-CSIA) in biological materials. *J. Anal. At.*
341 *Spectrom.* **2013**, *28*, 1620-1628, DOI: 10.1039/c3ja50185j.
- 342 (20) Rosera, T. J.; Janssen, S. E.; Tate, M. T.; Lepak, R. F.; Ogorek, J. M.; DeWild, J. F.; Babiarz, C. L.;
343 Krabbenhoft, D. P.; Hurley, J. P. Isolation of methylmercury using distillation and anion-exchange
344 chromatography for isotopic analyses in natural matrices. *Anal. Bioanal. Chem.* **2020**, *412*, 681–
345 690, DOI: 10.1007/s00216-019-02277-0.
- 346 (21) Manceau, A.; Bustamante, P.; Haouz, A.; Bourdineaud, J. P.; Gonzalez-Rey, M.; Lemouchi, C.;
347 Gautier-Luneau, I.; Geertsen, V.; Barriet, E.; Rovezzi, M.; Glatzel, P.; Pin, S. Mercury(II) binding to
348 metallothionein in *Mytilus Edulis* revealed by high energy-resolution XANES spectroscopy. *Chem.*
349 *Eur. J.* **2019**, *25*, 997, DOI: 10.1002/chem.201804209.
- 350 (22) Manceau, A.; Gaillot, A. C.; Glatzel, P.; Cherel, Y.; Bustamante, P. *In Vivo* formation of HgSe
351 nanoparticles and Hg-tetraselenolate complex from methylmercury in seabird – Implications for
352 the Hg-Se antagonism. *Environ. Sci. Technol.* **2021**, *55*, 1515-1526, DOI: 10.1021/acs.est.0c06269.
- 353 (23) Manceau, A.; Enescu, M.; Simionovici, A.; Lanson, M.; Gonzalez-Rey, M.; Rovezzi, M.; Tucoulou,
354 R.; Glatzel, P.; Nagy, K. L.; Bourdineaud, J. P. Chemical forms of mercury in human hair reveal
355 sources of exposure. *Environ. Sci. Technol.* **2016**, *50*, 10721-10729, DOI:
356 10.1021/acs.est.6b03468.
- 357 (24) Gajdosechova, Z.; Lawan, M. M.; Urgast, D. S.; Raab, A.; Scheckel, K. G.; Lombi, E.; Kopittke, P. M.;
358 Loeschner, K.; Larsen, E. H.; Woods, G.; Brownlow, A.; Read, F. L.; Feldmann, J.; Krupp, E. M. In
359 vivo formation of natural HgSe nanoparticles in the liver and brain of pilot whales. *Sci. Rep.* **2016**,
360 *6*, 34361, DOI: 10.1038/srep34361.
- 361 (25) Nakazawa, E.; Ikemoto, T.; Hokura, A.; Terada, Y.; Kunito, T.; Tanabe, S.; Nakai, I. The presence of
362 mercury selenide in various tissues of the striped dolphin: Evidence from μ -XRF-XRD and XAFS
363 analyses. *Metallomics* **2011**, *3*, 719–725, DOI: 10.1039/C0MT00106F.
- 364 (26) Arai, T.; Ikemoto, T.; Hokura, A.; Terada, Y.; Kunito, T.; Tanabe, S.; Nakai, I. Chemical forms of
365 mercury and cadmium accumulated in marine mammals and seabirds as determined by XAFS

- 366 analysis. *Environ. Sci. Technol.* **2004**, *38*, 6468-6474, DOI: 10.1021/es040367u.
- 367 (27) Hartman, C. A.; Ackerman, J. T.; Herzog, M. P.; Eagles-Smith, C. A. Season, molt, and body size
368 influence mercury concentrations in grebes. *Environ. Pollut.* **2017**, *229*, 29-39, DOI:
369 10.1016/j.envpol.2017.05.058.
- 370 (28) Ackerman, J. T.; Eagles-Smith, C. A.; Takekawa, J. Y.; Bluso, J. D.; Adelsbach, T. L. Mercury
371 concentrations in blood and feathers of prebreeding Forster's terns in relation to space use of
372 San Francisco Bay, California, USA, Habitats. *Environ. Toxicol. Chem.* **2008**, *27*, 897-908, DOI:
373 10.1897/07-230.1.
- 374 (29) Poulin, B. A.; Manceau, A.; Krabbenhoft, D. P.; Stewart, A. R.; Ward-Deitrich, C.; del Castillo Busto,
375 M. E.; Goenaga-Infante, H.; Bustamante, P. Mercury and selenium chemical characteristics and
376 speciation data of bird, fish, and earthworm tissues. *U.S. Geological Survey Data Release* **2020**,
377 DOI: 10.5066/P96NP376.
- 378 (30) Rovezzi, M.; Lapras, C.; Manceau, A.; Glatzel, P.; Verbeni, R. High energy-resolution X-ray
379 spectroscopy at ultra-high dilution with spherically bent crystal analyzers of 0.5 m radius. *Rev.*
380 *Sci. Instrum.* **2017**, *88*, 013108, DOI: 10.1063/1.4974100.
- 381 (31) Mah, V.; Jalilehvand, F. Glutathione complex formation with mercury(II) in aqueous solution at
382 physiological pH. *Chem. Res. Toxicol.* **2010**, *23*, 1815-1823, DOI: 10.1021/tx100260e.
- 383 (32) Manceau, A.; Wang, J.; Rovezzi, M.; Glatzel, P.; Feng, X. Biogenesis of mercury-sulfur
384 nanoparticles in plant leaves from atmospheric gaseous mercury. *Environ. Sci. Technol.* **2018**, *52*,
385 3935-3948, DOI: 10.1021/acs.est.7b05452.
- 386 (33) Kleckner, A. E.; Kakouros, E.; Robin Stewart, A. A practical method for the determination of total
387 selenium in environmental samples using isotope dilution-hydride generation-inductively
388 coupled plasma-mass spectrometry. *Limnol. Oceanogr. Methods* **2017**, *15*, 363-371, DOI:
389 10.1002/lom3.10164.
- 390 (34) Janssen, S. E.; Lepak, R. F.; Tate, M. T.; Ogorek, J. M.; DeWild, J. F.; Babiarez, C. L.; Hurley, J. P.;
391 Krabbenhoft, D. P. Rapid pre-concentration of mercury in solids and water for isotopic analysis.
392 *Anal. Chim. Acta* **2019**, *1054*, 95-103, DOI: 10.1016/j.aca.2018.12.026.
- 393 (35) Yin, R.; Krabbenhoft, D. P.; Bergquist, B. A.; Zheng, W.; Lepak, R. F.; Hurley, J. P. Effects of
394 mercury and thallium concentrations on high precision determination of mercury isotopic
395 composition by Neptune Plus multiple collector inductively coupled plasma mass spectrometry. *J.*
396 *Anal. At. Spectrom.* **2016**, *31*, 2060-2068, DOI: 10.1039/c6ja00107f.
- 397 (36) Thomas, S. A.; Mishra, B.; Myneni, S. C. B. Cellular mercury coordination environment, and not
398 cell surface ligands, influence bacterial methylmercury production. *Environ. Sci. Technol.* **2020**,
399 *54*, 3960-3968, DOI: 10.1021/acs.est.9b05915.
- 400 (37) Bergquist, B. A.; Blum, J. D. Mass-dependent and -independent fractionation of Hg isotopes by
401 photoreduction in aquatic systems. *Science* **2007**, *318*, 417-420, DOI: 10.1126/science.1148050.
- 402 (38) Perrot, V.; Pastukhov, M. V.; Epov, V. N.; Husted, S.; Donard, O. F. X.; Amouroux, D. Higher mass-
403 independent isotope fractionation of methylmercury in the pelagic food web of Lake Baikal
404 (Russia). *Environ. Sci. Technol.* **2012**, *46*, 5902-5911, DOI: 10.1021/es204572g.
- 405 (39) Mariotti, A.; Germon, J. C.; Hubert, P.; Kaiser, P.; Letolle, R.; Tardieux, A.; Tardieux, P.

- 406 Experimental determination of nitrogen kinetic isotope fractionation: Some principles;
407 illustration for the denitrification and nitrification processes. *Plant Soil* **1981**, *62*, 413-430, DOI:
408 10.1007/BF02374138.
- 409 (40) York, D. Least-squares fitting of a straight line. *Can. J. Phys.* **1966**, *44*, 1079–1086, DOI:
410 10.1139/p66-090.
- 411 (41) Burk, R. F.; Hill, K. E. Selenoprotein P-expression, functions, and roles in mammals. *Biochim.*
412 *Biophys. Acta* **2009**, 1790, 1441-1447, DOI: 10.1016/j.bbagen.2009.03.026.
- 413 (42) Khan, M. A. K.; Wang, F. Chemical demethylation of methylmercury by selenoamino acids. *Chem.*
414 *Res. Toxicol.* **2010**, *23*, 1202-1206, DOI: 10.1021/tx100080s.
- 415 (43) Asaduzzaman, A. M.; Schreckenbach, G. Degradation mechanism of methyl mercury selenoamino
416 acid complexes: A computational study. *Inorg. Chem.* **2011**, *50*, 2366-2372, DOI:
417 10.1021/ic1021406.
- 418 (44) Kritee, K.; Barkay, T.; Blum, J. D. Mass dependent stable isotope fractionation of mercury during
419 *mer* mediated microbial degradation of monomethylmercury. *Geochim. Cosmochim. Acta* **2009**,
420 *73*, 1285-1296, DOI: 10.1016/j.gca.2008.11.038.
- 421 (45) Penglase, S.; Hamre, K.; Ellingsen, S. The selenium content of SEPP1 versus selenium
422 requirements in vertebrates. *PeerJ* **2015**, *3*, e1244, DOI: 10.7717/peerj.1244.
- 423 (46) Pickering, I. J.; Cheng, Q.; Rengifo, E. M.; Nehzati, S.; Dolgova, N. V.; Kroll, T.; Sokaras, D.; George,
424 G. N.; Arnér, E. S. J. Direct observation of methylmercury and auranofin binding to selenocysteine
425 in thioredoxin reductase. *Inorg. Chem.* **2020**, *59*, 2711-2718, DOI:
426 10.1021/acs.inorgchem.9b03072.
- 427 (47) Yamashita, Y.; Yamashita, M. Identification of a novel selenium-containing compound,
428 selenoneine, as the predominant chemical form of organic selenium in the blood of bluefin tuna.
429 *J. Biol. Chem.* **2010**, *285*, 18134-18138, DOI: 10.1074/jbc.C110.106377.
- 430 (48) Renedo, M.; Amouroux, D.; Duval, B.; Carravieri, A.; Tessier, E.; Barre, J.; Bérail, S.; Pedrero, Z.;
431 Cherel, Y.; Bustamante, P. Seabird tissues as efficient biomonitoring tools for Hg isotopic
432 investigations: Implications of using blood and feathers from chicks and adults. *Environ. Sci.*
433 *Technol.* **2018**, *52*, 4227-4234, DOI: 10.1021/acs.est.8b00422.
- 434 (49) Seewagen, C. L.; Cristol, D. A.; Gerson, A. R. Mobilization of mercury from lean tissues during
435 simulated migratory fasting in a model songbird. *Sci. Rep.* **2016**, *6*, 25762, DOI:
436 10.1038/srep25762.
- 437 (50) Ewald, J. D.; Kirk, J. L.; Li, M.; Sunderland, E. M. Organ-specific differences in mercury speciation
438 and accumulation across ringed seal (*Phoca hispida*) life stages. *Sci. Total Environ.* **2019**, *650*,
439 2013-2020, DOI: 10.1016/j.scitotenv.2018.09.299.
- 440 (51) Sherman, L. S.; Blum, J. D.; Franzblau, A.; Basu, N. New insight into biomarkers of human mercury
441 exposure using naturally occurring mercury stable isotopes. *Environ. Sci. Technol.* **2013**, *47*, 3403-
442 3409, DOI: 10.1021/es305250z.
- 443 (52) Laffont, L.; Sonke, J. E.; Maurice, L.; Monrroy, S. L.; Chincheros, J.; Amouroux, D.; Behra, P. Hg
444 speciation and stable isotope signatures in human hair as a tracer for dietary and occupational
445 exposure to mercury. *Environ. Sci. Technol.* **2011**, *45*, 9910-9916, DOI: 10.1021/es202353m.

446 (53) Wiederhold, J. G.; Cramer, C. J.; Daniel, K.; Infante, I.; Bourdon, B.; Kretzschmar, R. Equilibrium
447 mercury isotope fractionation between dissolved Hg(II) species and thiol-bound Hg. *Environ. Sci.*
448 *Technol.* **2010**, *44*, 4191–4197, DOI: 10.1021/es100205t.

449 (54) Bearhop, S.; Ruxton, G. D.; Furness, R. W. Dynamics of mercury in blood and feathers of great
450 skuas. *Environ. Toxicol. Chem.* **2000**, *19*, 1638-1643, DOI: 10.1002/etc.5620190622.

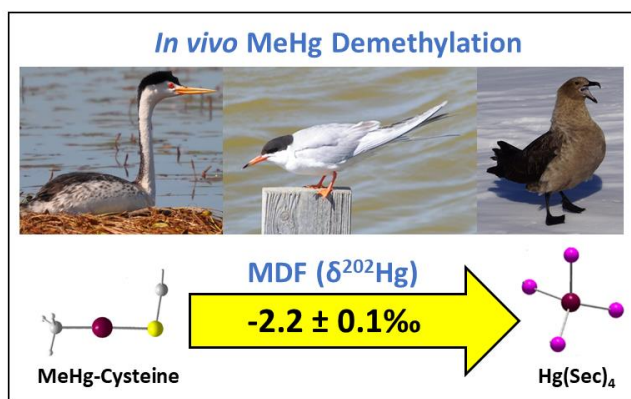
451

452

453

454

455 **TOC Art**



456

457

458

459

460

461

462 **Figures and Tables**

463 **Table 1.** Chemical, spectroscopic, and isotopic data of bird tissue and feather samples.

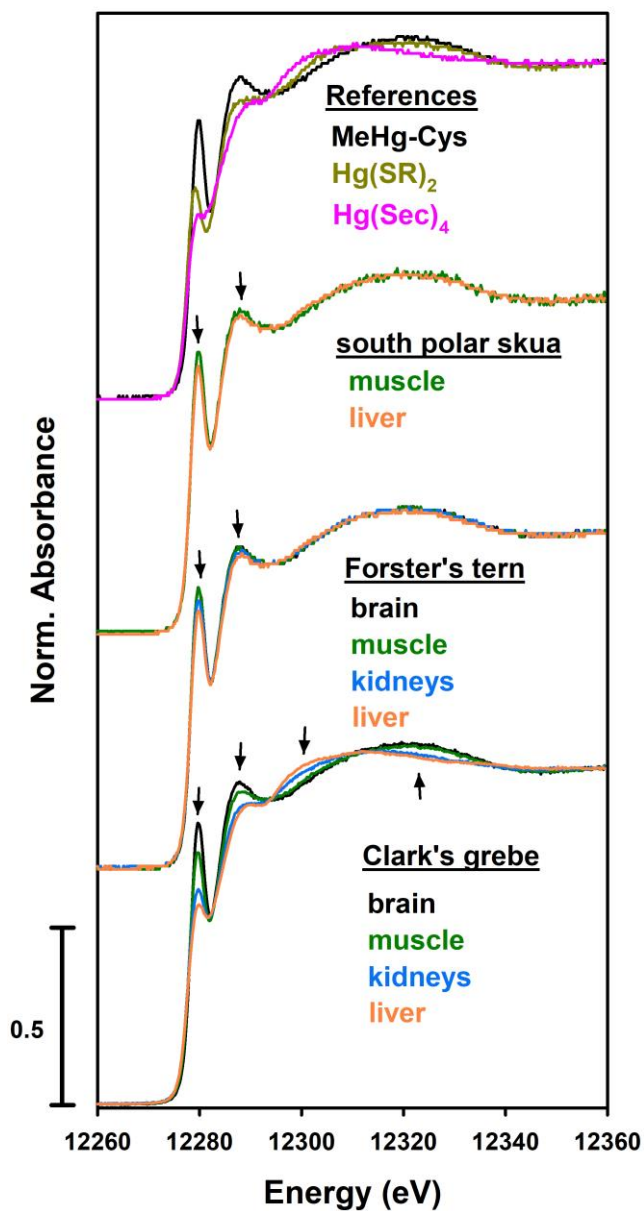
Tissue	----- Chemical Meas. ----- ^a			----- HR-XANES fit results ----- ^b			----- Species-specific isotope ratios -----			
	THg (mg/kg)	MeHg (mg/kg)	Se (mg/kg)	%MeHg-Cys	%Hg(Sec) ₄	%Hg(SR) ₂	δ ²⁰² THg (±1SD)	Δ ¹⁹⁹ THg (±1SD)	δ ²⁰² MeHg (±1SD)	Δ ¹⁹⁹ MeHg (±1SD)
Clark's grebe (<i>A. clarkii</i>)										
Brain	3.18	2.98	1.55	100	0	0	0.07 (0.03)	1.51 (0.03)	0.06 (0.04)	1.49 (0.02)
Muscle	7.10	3.71	2.31	66	11	23	-1.13 (0.04)	1.46 (0.04)	-0.22 (0.03)	1.43 (0.02)
Kidneys	21.6	6.38	10.6	28	59	12	-1.41 (0.03)	1.42 (0.04)	0.14 (0.02)	1.45 (0.03)
Liver	43.1	7.86	19.3	14	86	0	-2.07 (0.04)	1.49 (0.04)	-0.17 (0.02)	1.42 (0.02)
Breast Feather	41.4	32.7	1.04	100	0	0	0.15 (0.03)	1.77 (0.02)	0.13 (0.05)	2.04 (0.03)
Forster's tern (<i>S. forsteri</i>)										
Brain	5.28	4.48	3.31	100	0	0	0.51 (0.02)	0.68 (0.02)	0.57 (0.01)	0.81 (0.02)
Muscle	6.39	5.65	3.33	100	0	0	0.53 (0.03)	0.72 (0.03)	0.31 (0.02)	0.79 (0.02)
Kidneys	12.6	9.21	9.64	85	15	0	0.34 (0.02)	0.70 (0.03)	0.62 (0.03)	0.66 (0.02)
Liver	13.8	9.22	6.21	75	25	0	-0.14 (0.02)	0.67 (0.03)	0.45 (0.04)	0.71 (0.08)
Breast Feather	28.6	18.2	1.41	100	0	0	0.70 (0.03)	1.65 (0.04)	0.72 (0.02)	1.81 (0.04)
south polar skua (<i>S. maccormicki</i>)										
Muscle	1.75	1.39	19.4	100	0	0	1.25 (0.05)	1.99 (0.03)	--	--
Kidneys	8.61	4.56	--	--	--	--	0.17 (0.03)	2.00 (0.05)	1.25 (0.01)	1.92 (0.01)
Liver	8.19	6.39	29.7	83	17	0	0.80 (0.01)	2.02 (0.04)	--	--
^a reported on a dry weight basis.										
^b precision of fit results are 5% for the Clark's grebe tissues ⁴ and 10% for Forster's tern and south polar skua tissues (see SI Table S2).										

464

465

466

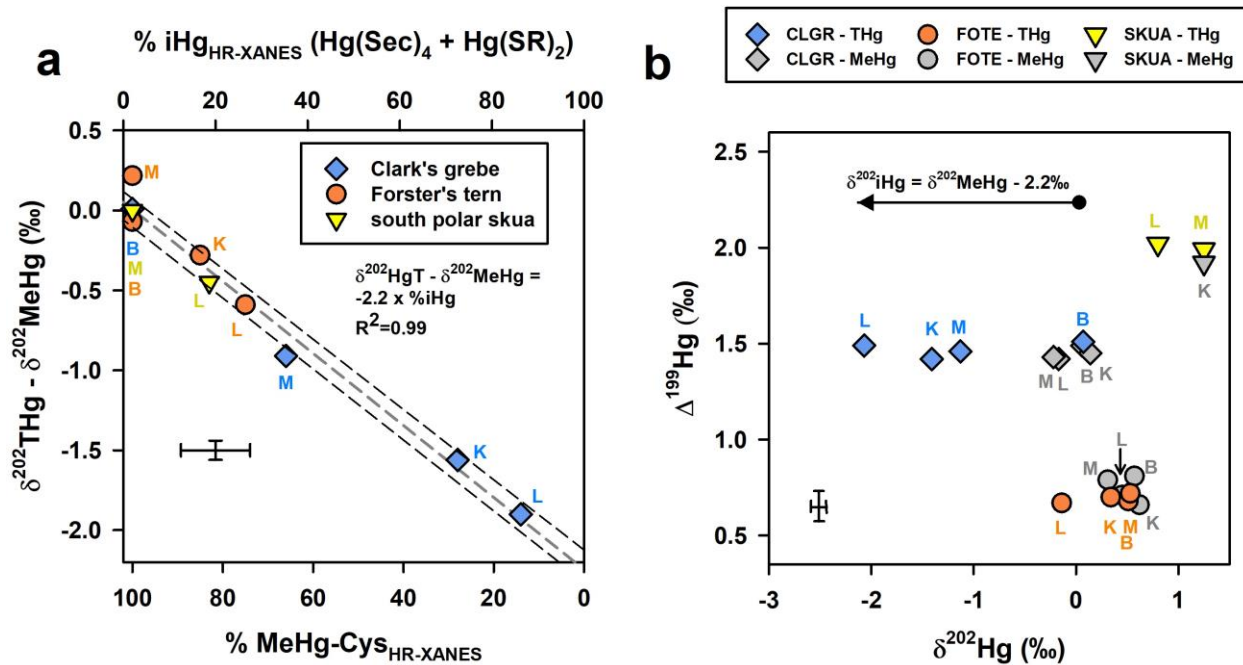
467



468
 469 **Figure 1.** Hg L₃-edge HR-XANES spectra of tissues from a Clark's grebe, Forster's tern, and south polar skua (brain,
 470 black; muscle, green; kidneys, blue; liver, orange). Black arrows identify regions of the spectra that differ with
 471 shifts in mercury speciation primarily in the proportion of MeHg-Cys and Hg(Sec)₄. References spectra are shown
 472 for the three species observed in the tissues (MeHg-Cys; Hg(SR)₂; Hg(Sec)₄).

473
 474
 475
 476
 477

478
 479
 480
 481
 482



483
 484 **Figure 2.** (a) Relationship between the difference in $\delta^{202}\text{Hg}$ values of total mercury minus methylmercury ($\delta^{202}\text{THg}$
 485 $-\delta^{202}\text{MeHg}$; Table 1) and the speciation of mercury as determined by HR-XANES of bird tissues; data are weighted
 486 to uncertainties of both X and Y variables. (b) Biplot of $\Delta^{199}\text{Hg}$ versus $\delta^{202}\text{Hg}$ of total mercury (THg; color-filled
 487 symbols) and methylmercury (MeHg; gray-filled symbols) for bird tissues. Single letters abbreviations identify the
 488 tissue type (B, brain; K, kidneys; L, liver; M, muscle). Generic error bars present uncertainties of isotope
 489 measurements (2SD) and HR-XANES fits (Table S2). In plot a the dashed gray and black lines present the fit of data
 490 and 95% confidence interval of the fit, respectively.